Missouri University of Science and Technology

Scholars' Mine

Electrical and Computer Engineering Faculty Research & Creative Works

Electrical and Computer Engineering

01 Jan 2023

Three-Terminal Noise Source Extraction From A Qi-Based Wireless Power Transfer System For Predicting Conducted Emissions

Srinath Penugonda

Siqi Bai

Varittha Sanphuang

Nevin Altunyurt

et. al. For a complete list of authors, see https://scholarsmine.mst.edu/ele_comeng_facwork/5082

Follow this and additional works at: https://scholarsmine.mst.edu/ele_comeng_facwork

 Part of the Electrical and Computer Engineering Commons

Recommended Citation

S. Penugonda et al., "Three-Terminal Noise Source Extraction From A Qi-Based Wireless Power Transfer System For Predicting Conducted Emissions," *IEEE Transactions on Electromagnetic Compatibility*, Institute of Electrical and Electronics Engineers, Jan 2023.
The definitive version is available at https://doi.org/10.1109/TEMC.2023.3296639

This Article - Journal is brought to you for free and open access by Scholars' Mine. It has been accepted for inclusion in Electrical and Computer Engineering Faculty Research & Creative Works by an authorized administrator of Scholars' Mine. This work is protected by U. S. Copyright Law. Unauthorized use including reproduction for redistribution requires the permission of the copyright holder. For more information, please contact scholarsmine@mst.edu.

This article has been accepted for inclusion in a future issue of this journal. Content is final as presented, with the exception of pagination.

Three-Terminal Noise Source Extraction From a Qi-Based Wireless Power Transfer System for Predicting Conducted Emissions

Srinath Penugonda, *Student Member, IEEE*, Siqi Bai, *Student Member, IEEE*, Varittha Sanphuang, *Member, IEEE*, Nevin Altunyurt, *Member, IEEE*, Hongseok Kim, *Member, IEEE*, Daryl Beetner, *Senior Member, IEEE*, and Jun Fan, *Fellow, IEEE*

***Abstract*—An equivalent method to extract a three-terminal noise source from a Qi-based wireless power transfer system is proposed in this article. This method is capable of extracting a source for both the positive (P) and negative (N) lines with respect to the third terminal (the ground chassis or reference plane). The extracted sources are independent of the setup configuration and can be used to predict currents or voltages on the P and N lines on a setup that is different from the extraction setup. In the following article, a three-terminal model independent of the setup configuration is first extracted. The extracted sources are then verified by predicting currents on a setup that is different from the original setup (such as a different load impedance and height of the device above reference plane). Finally, the extracted sources are used to predict the voltages on a 1-m cable harness. The predicted currents and voltages agree within 5 dB against measurement data over a frequency range from 0.5 to 30 MHz. The proposed method can be used to predict currents and voltages on any power converter with a single-phase input configuration.**

***Index Terms*—Black-box modeling, common-mode impedance, equivalent source extraction, single-ended current prediction, terminal modeling, wireless power transfer (WPT).**

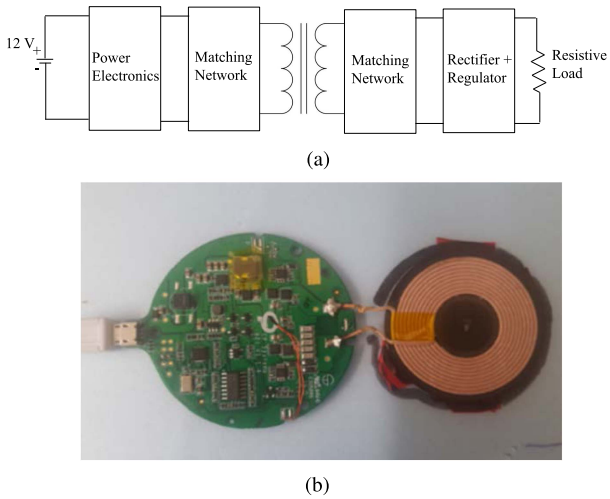

Fig. 1. WPT module considered. (a) Block diagram of the WPT where power electronics represents buck converter and full-bridge inverter. (b) Actual WPT used as the DUT (receiver and resistive load not shown).

I. Introduction

WIRELESS power transfer (WPT) technology has become popular in the past decade as a method to charge various consumer electronic devices [1]. A block diagram and a photo of the WPT system being considered as a device under test (DUT) in this article is shown in Fig. 1. The WPT system consists of a transmitter and a receiver. The transmitter has a buck converter, a full-bridge inverter, and a transmitting coil. The receiver contains a receiving coil, rectifier, dc-converter (direct current), and a resistive load. The inevitable high $\mathrm{d}v/\mathrm{d}t$ and $\mathrm{d}i/\mathrm{d}t$ switching of power converters (the buck converter and full-bridge inverter in the DUT) may cause electromagnetic interference (EMI) issues [2].

The stochastic behavior of the switch-mode power supplies and power converters [1] introduces complexity for modeling these systems from the perspective of EMI analysis. While SPICE circuit models or a hybrid solution using SPICE and a full-wave solver provides a solution for predicting the EMI from the power converters, these models require a considerable amount of time to build and are still likely to have an accuracy issue due to lack of information about some components, such as an integrated circuit component for sensing and control or a semiconductor chip. On the other hand, a terminal/black-box model can be developed relatively fast with sufficient accuracy for certain operating conditions. Moreover, a terminal modeling technique does not require prior knowledge of circuit schematics and internal coupling mechanisms, while the EMI modeling technique based on SPICE and/or electromagnetic field solver does.

Terminal models based on Thevenin or Norton equivalents have been discussed and developed in many works of literature

Manuscript received 13 December 2021; revised 9 July 2022, 9 October 2022, and 20 December 2022; accepted 21 March 2023. This work was supported by the National Science Foundation (NSF) under Grant IIP-1916535. *(Corresponding author: Srinath Penugonda.)*

Srinath Penugonda, Siqi Bai, Hongseok Kim, Daryl Beetner, and Jun Fan are with the Missouri University of Science and Technology, Rolla, MO 65409 USA (e-mail: penugondasrinath@gmail.com; sb2pc@mst.edu; kimhong@mst.edu; daryl@mst.edu; jfan@mst.edu).

Varittha Sanphuang and Nevin Altunyurt are with the Ford Motor Company, Dearborn, MI 48121 USA (e-mail: vsanphua@ford.com; naltunyu@ford.com).

Color versions of one or more figures in this article are available at https://doi.org/10.1109/TEMC.2023.3296639.

Digital Object Identifier 10.1109/TEMC.2023.3296639

0018-9375 © 2023 IEEE. Personal use is permitted, but republication/redistribution requires IEEE permission.
See https://www.ieee.org/publications/rights/index.html for more information.

Authorized licensed use limited to: Missouri University of Science and Technology. Downloaded on August 29,2023 at 13:58:31 UTC from IEEE Xplore. Restrictions apply.

This article has been accepted for inclusion in a future issue of this journal. Content is final as presented, with the exception of pagination.

in the past. In a terminal modeling method, each terminal of a switch noise source is replaced with an equivalent voltage or a current source in series or parallel to a equivalent noise source impedance. Bishnoi et al. [3] described a multiterminal mode but fail to discuss a setup-independent model. Baisden [4] also introduced a "generalized" three-terminal model but also failed to address the need for extraction of a setup-independent source information. In [5], the approach for extracting the terminal model is different from that of [3]. Instead of using single-ended sources for representing noises like in [3] and many other research articles [4], [5], [6], [7], [8], [9], [10], the differential-mode (DM) and common-mode (CM) noise sources were used in [5]. The major drawback of using DM and CM noise sources is that there is always an inevitable mixed-mode (MM) noise (noise conversion between DM to CM and vice versa). Bishnoi et al. [6] used a similar approach of using DM and CM sources to represent the noise, but also falls short of addressing the abovementioned limitations. In [7] and [8], the authors use black-box models of buck/boost converters to estimate radiated emissions, but require that the setup used to extract the sources (i.e., height of the converter and attached cables above the ground plane) is the same as the one used to predict emissions. This requirement limits the usage of an extracted source in different testing or usage scenarios. Unlike the abovementioned research articles where the extracted source information is used on the same setup configuration, PÉrez et al. [9] applied the sources extracted from the terminal modeling technique on a different setup than is used to extract the sources, but still uses MM noise sources.

This article proposes a methodology to extract a setup-independent three-terminal black-box model of a power converter. The extracted black-box model of the DUT using the proposed methodology can be used to predict conducted noise voltages and currents under various testing conditions that are different from the reference setup where the model is extracted and does not exhibit the aforementioned limitations from the previous research articles. The rest of this article is organized as follows. Section II introduces the methodology for extracting the three-terminal source information for a Qi-based WPT system that is independent of the setup configuration. In Section III, the measurement setup for extracting the source information is explained and the three-terminal model of the DUT is extracted using a time-domain technique similar to the one presented in [10]. In section IV, the extracted model from Section III is verified on a setup configuration that is different from the original setup presented in Section III. Section V discusses the limitations under which extracted sources are valid. Finally, Section VI concludes this article.

II. Methodology for Extracting a Three-Terminal Model

In the CM Thevenin equivalent model discussed in [10], the WPT system was replaced with a voltage source, Vth in series with its impedance, Zth. For the three-terminal source model, the WPT system is replaced with voltage sources on the positive (P) and on the negative (N) lines, V_P and V_N, respectively.

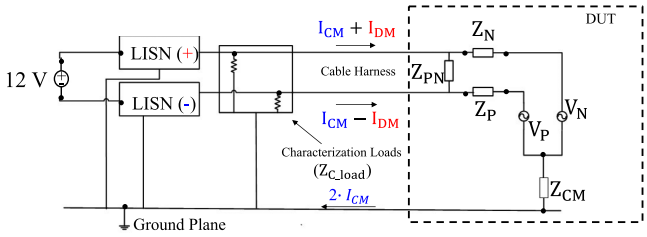

Fig. 2. Block diagram showing the equivalent three-terminal noise source model.

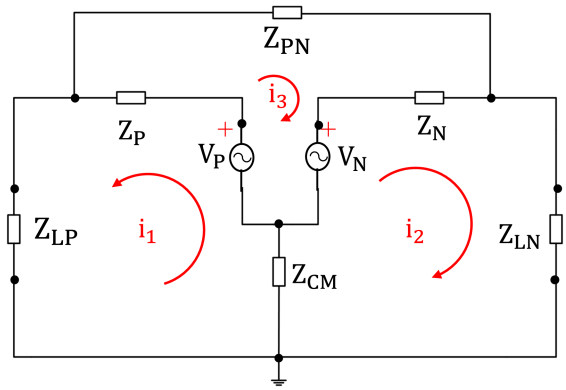

Fig. 3. Simplified circuit used for the equivalent source extraction method.

The source impedances Z_P and Z_N are placed in series with the voltage sources, as shown in Fig. 2. The three-terminal noise source model also contains a mutual impedance Z_{PN} to include the mutual coupling between the P and N lines. The three-terminal model described in this article also has a shared CM impedance Z_{CM}. The impedance Z_{CM} is the impedance between the switching node of the DUT and the nearest ground (GND) plane. In a typical CISPR-25 standard, the GND chassis of the DUT is connected to the table GND with a metallic strap. In this article, the strap is considered. The process of extracting source information described in this article is the same whether a metallic strap is present or not. For example, if there is a metallic strap between the DUT chassis and the reference ground plane, an impedance, Z_{strap}, would be placed in series to the Z_{CM}, as shown in Fig. 2. The impedance Z_{CM} facilitates the flow of CM current, I_{CM}, to the ground plane. The DUT is connected to a line impedance stabilization network (LISN) on each of the lines through a cable harness or a universal serial bus (USB) cable.

The source information V_P, V_N, Z_P, Z_N, and Z_{PN} can be extracted by forming a system of equations using Kirchoff's current law (KCL). For ease of applying KCL, the block diagram in Fig. 2 is reduced to Fig. 13. The load impedances Z_LP and Z_LN on the P and N lines, respectively, represent the parallel combination of the characterization load Z_{c_load} and LISN impedances Z_{LISN_P} and Z_{LISN_N}. The characterization load impedance is connected in shunt with the LISN impedance to change the impedance of the DUT looking toward the LISNs. The characterization impedance can be different for P and N lines, $Z_{C\_load\_P}$, $Z_{C\_load\_N}$, where suffixes "_P" and "_N" represent P and N lines, respectively. Equations (1) and (2) are derived by applying KCL to the circuit in Fig. 3. Equations (3) and

Authorized licensed use limited to: Missouri University of Science and Technology. Downloaded on August 29,2023 at 13:58:31 UTC from IEEE Xplore. Restrictions apply.

This article has been accepted for inclusion in a future issue of this journal. Content is final as presented, with the exception of pagination.

(4) are

$$V_{\mathrm{P}} - Z_{\mathrm{P}} i_1 - (i_1 Z_{\mathrm{LP}} - i_2 Z_{\mathrm{LN}}) \frac{Z_{\mathrm{P}}}{Z_{\mathrm{PN}}} - Z_{\mathrm{LP}} i_1 - Z_{\mathrm{CM}}(i_1 + i_2) = 0 \quad (1)$$

$$V_{\mathrm{N}} - Z_{\mathrm{N}} i_2 + (i_1 Z_{\mathrm{LP}} - i_2 Z_{\mathrm{LN}}) \frac{Z_{\mathrm{N}}}{Z_{\mathrm{PN}}} - Z_{\mathrm{LN}} i_2 - Z_{\mathrm{CM}}(i_1 + i_2) = 0 \quad (2)$$

$$V_{\mathrm{P}} - i_1 \left(Z_{\mathrm{P}} + \frac{Z_{\mathrm{P}} Z_{\mathrm{LP}}}{Z_{\mathrm{PN}}} + Z_{LP} + Z_{\mathrm{CM}} \right) - i_2 \left(Z_{\mathrm{CM}} - \frac{Z_{\mathrm{P}} Z_{\mathrm{LN}}}{Z_{\mathrm{PN}}} \right) = 0 \quad (3)$$

$$V_{\mathrm{N}} - i_2 \left(Z_{\mathrm{N}} + \frac{Z_{\mathrm{N}} Z_{\mathrm{LN}}}{Z_{\mathrm{PN}}} + Z_{\mathrm{LN}} + Z_{\mathrm{CM}} \right) - i_1 \left(Z_{\mathrm{CM}} - \frac{Z_{\mathrm{N}} Z_{\mathrm{LP}}}{Z_{\mathrm{PN}}} \right) = 0 \quad (4)$$

derived from (1) and (2). The currents i_1 and i_2 are flowing through P and N lines and returning on the ground plane. These currents, as well as the Z_{CM}, are obtained through measurements, as shown in Section III. Hence, in (3) and (4), there are five unknowns: $V_{\mathrm{P}}, V_{\mathrm{N}}, Z_{\mathrm{P}}, Z_{\mathrm{N}}$, and Z_{PN}. Each measurement produces two equations: a set of (3) and (4). Therefore, to solve for five unknowns, three measurements are required. The measurements are performed by varying a combination or $Z_{\mathrm{c\_load}}$ and Z_{CM} [see (5)–(8)]. Equations (3) and (4) are coupled nonlinear equations. A least-square nonlinear solver `lsqnonlin` [11] available in MATLAB was used to solve for these unknowns. The setup-dependent Z_{CM} was also chosen as a variable so that the equivalent source information could be extracted independent of the setup configuration. In (5)–(8), Z'_{LP}, Z'_{LN}, and Z'_{CM} represent the change in the corresponding variable. While Z'_{LP} and Z'_{LN} are obtained by adding a shunt impedance to the default LISN impedance, Z'_{CM} represents the CM impedance of the DUT from the ground plane at a height H_2 [assuming the DUT is placed at a height H_1 in (3) and (4)]. The currents measured related to the abovementioned setup changes are i_3, i_4 and i_5, i_6 respectively.

$$V_{\mathrm{P}} - i_3 \left(Z_{\mathrm{P}} + \frac{Z_{\mathrm{P}} Z'_{\mathrm{LP}}}{Z_{\mathrm{PN}}} + Z'_{\mathrm{LP}} + Z_{\mathrm{CM}} \right) - i_4 \left(Z_{\mathrm{CM}} - \frac{Z_{\mathrm{P}} Z'_{\mathrm{LN}}}{Z_{\mathrm{PN}}} \right) = 0 \quad (5)$$

$$V_{\mathrm{N}} - i_4 \left(Z_{\mathrm{N}} + \frac{Z_{\mathrm{N}} Z'_{\mathrm{LN}}}{Z_{\mathrm{PN}}} + Z'_{\mathrm{LN}} + Z_{\mathrm{CM}} \right) - i_3 \left(Z_{\mathrm{CM}} - \frac{Z_{\mathrm{N}} Z'_{\mathrm{LP}}}{Z_{\mathrm{PN}}} \right) = 0 \quad (6)$$

$$V_{\mathrm{P}} - i_5 \left(Z_{\mathrm{P}} + \frac{Z_{\mathrm{P}} Z_{\mathrm{LP}}}{Z_{\mathrm{PN}}} + Z_{\mathrm{LP}} + Z'_{\mathrm{CM}} \right) - i_6 \left(Z'_{\mathrm{CM}} - \frac{Z_{\mathrm{P}} Z_{\mathrm{LN}}}{Z_{\mathrm{PN}}} \right) = 0 \quad (7)$$

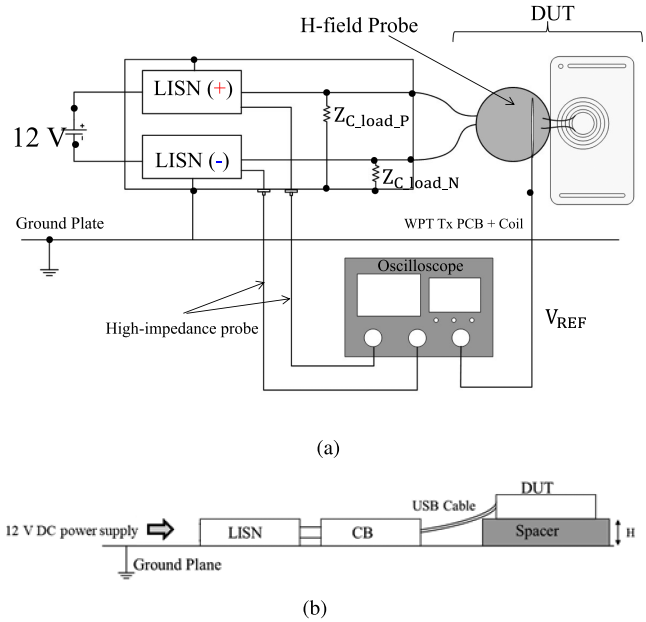

Fig. 4. Block diagram of the setup. (a) Measurement used for the three terminal model extraction. (b) Side view of various blocks.

$$V_{\mathrm{N}} - i_6 \left(Z_{\mathrm{N}} + \frac{Z_{\mathrm{N}} Z_{\mathrm{LN}}}{Z_{\mathrm{PN}}} + Z_{\mathrm{LN}} + Z'_{\mathrm{CM}} \right) - i_5 \left(Z'_{\mathrm{CM}} - \frac{Z_{\mathrm{N}} Z_{\mathrm{LP}}}{Z_{\mathrm{PN}}} \right) = 0. \quad (8)$$

III. Description of the Measurement Setup

The measurement setup for extracting the terminal model of the DUT consists of two LISNs with characterization loads on a characterization board, a micro-USB cable, a WPT transmitter, receiver module, a copper plate as a ground plane, an oscilloscope, and an H-field probe. Fig. 4(a) shows the detailed block diagram of the measurement setup and Fig. 4(b) shows the side view. As can be seen, the characterization board and WPT are connected in series using the micro-USB cable. A 12-V dc power supply (or a battery) powers the DUT. The WPT receiver is connected to a resistive load so that the state of the device being charged does not affect the operating conditions of the DUT. To correct the phases of the measured voltages on the P and N lines at different instances, a reference voltage (V_{REF}) is measured using the H-field probe. To obtain (5) and (6), the impedance $Z_{\mathrm{c\_load}}$ is changed on the characterization board. The characteristic load $Z_{\mathrm{c\_load}}$ is changed by modifying the shunt resistances on the P and N lines [see Fig. 5(a)]. The resistances are connected between the P and N lines and the GND of the characterization board (which in turn is connected to the ground plane) using a dc blocking capacitor (1 μF). A dc blocking capacitor prevents loading the power supply due to the impedance connected between the P and N lines and the ground plane. The impedance Z_{CM} is modified by changing the height of the DUT with respect to the ground plane, for example, modifying the height of the spacer H, as shown in Fig. 4(b), providing (7) and (8).

Authorized licensed use limited to: Missouri University of Science and Technology. Downloaded on August 29,2023 at 13:58:31 UTC from IEEE Xplore. Restrictions apply.

This article has been accepted for inclusion in a future issue of this journal. Content is final as presented, with the exception of pagination.

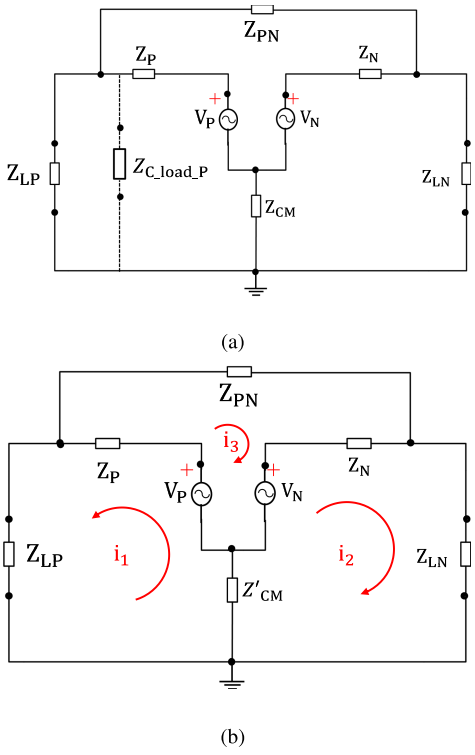

Fig. 5. Circuit diagram of the setup. (a) Load impedance modified by addition of $Z_{\text{c\_load}}$. (b) With modified CM impedance of DUT with respect to the ground plane Z'_{CM}.

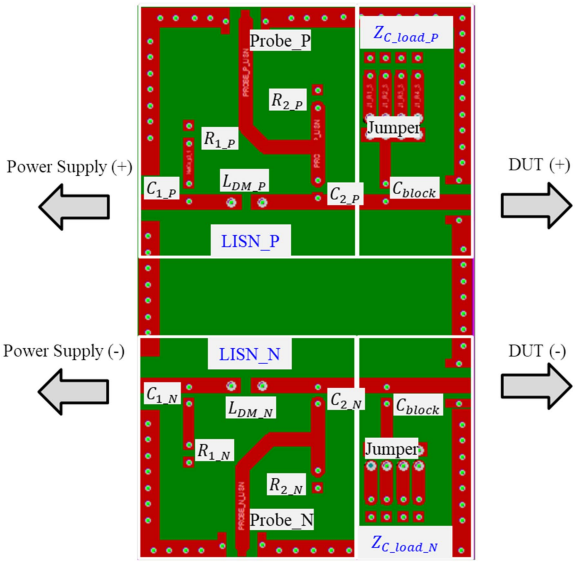

Fig. 6. Characteristic board with LISN + R_{load}.

A. Characterization Board With LISN

The characterization board consists of LISNs and characterization loads on both the P and N lines (see Fig. 6). The two LISNs connected to the P and N lines are identical. The LISN circuit diagram is shown in Fig. 7. A matrix of characterization loads present on the characterization board can be used to change the impedance on the P and N lines with respect to the ground plane. The loads can be changed by using the jumper between P and N lines and R_{load}. The characterization board also contains pads for probing the LISN output across the resistance R_2. High-impedance (1 MΩ, 10 : 1) probes are used to measure the voltages at the LISN output pads (Probe_P and Probe_N in Fig. 6). The voltages are then converted to currents that can be used in (1)–(8) using Ohm's law as follows:

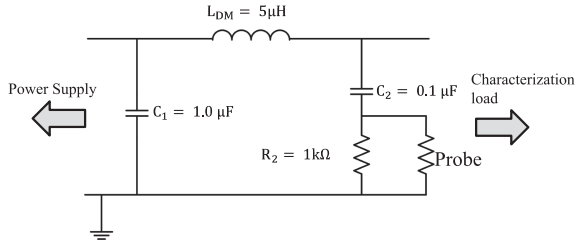

Fig. 7. Circuit diagram of the LISN.

$$I_{k\_\text{P}} = \frac{V_{k\_\text{P}}}{Z_{\text{LP}}} \tag{9}$$

$$I_{k\_\text{N}} = \frac{V_{k\_\text{N}}}{Z_{\text{LN}}} \tag{10}$$

where $k = 1, 2, 3 \ldots 6$.

B. Impedance Measurement of LISN + CB (Z^k_{LP}, Z^k_{LN}) and WPT (Z_{CM})

The single-ended impedances of both the P and N lines were measured separately and plugged back into (3)–(8). Single-ended impedances for both the P and N lines (Z_{LP}, Z_{LN}, Z'_{LP}, and Z'_{LN}) for both LISN and characterization board were measured with a two-port Keysight Vector Network Analyzer (VNA) E5071 C. The VNA was connected at Probe_P and Probe_N locations, as shown in Fig. 6. The measurement setup is shown in Fig. 8(a). The measurement was repeated with various $Z_{\text{C\_load}}$ impedances. This provides various Z_{LP} and Z_{LN} impedances to fill in (9) and (10). Values of $Z_{\text{C\_load}}$ used for this article are 50, 150, 350, and 450 Ω. It is important to note that in terminal modeling, the nonlinear switching of various devices on the DUT are characterized by linear elements, such as $V_{\text{P}}, V_{\text{N}}, Z_{\text{P}}, Z_{\text{N}}$, and Z_{PN} [3]. Hence, it is recommended to know the load impedance conditions the DUT would be subjected to in advance so that the extracted sources provide reasonable predictions. Also, the MM noise of the characterization board under different $Z_{\text{C\_load}}$ values have to be reduced. As can be observed from Fig. 8(b), both the P and N impedances are symmetric with respect to the ground since the P and N impedances agree within 1 Ω.

The CM impedance Z_{CM} of the DUT was measured using a similar setup as the one used for the measurement of Z_{LP} and Z_{LN}, but by connecting the P and N terminals of the micro-USB cable to the positive conductor of the VNA, as shown in Fig. 9(a). It is important to note that an open-ended co-axial cable is used to connect the VNA cable to the DUT. While performing, the VNA is calibrated with a low IF-bandwidth of 100 Hz with 64 averages. A total of 1601 frequency points logarithmically spaced between 100 kHz and 30 MHz were used. While measuring

Authorized licensed use limited to: Missouri University of Science and Technology. Downloaded on August 29,2023 at 13:58:31 UTC from IEEE Xplore. Restrictions apply.

This article has been accepted for inclusion in a future issue of this journal. Content is final as presented, with the exception of pagination.

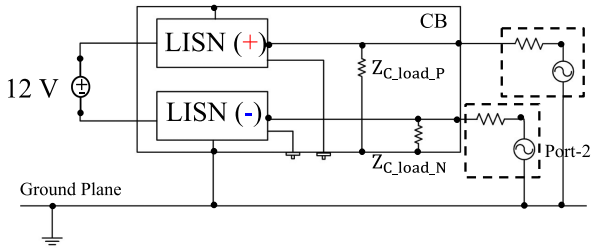

(a)

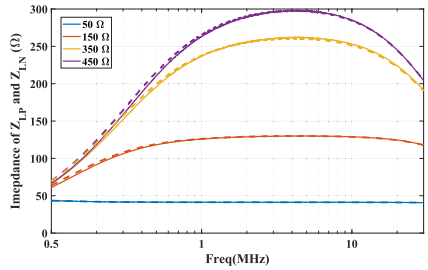

(b)

Fig. 8. Impedance measurement setups and results of LISN + CB. (a) Single-ended impedance measurement setup for P and N lines. (b) Measured impedances Z_{LP} (solid line) and Z_{LN} (dashed line).

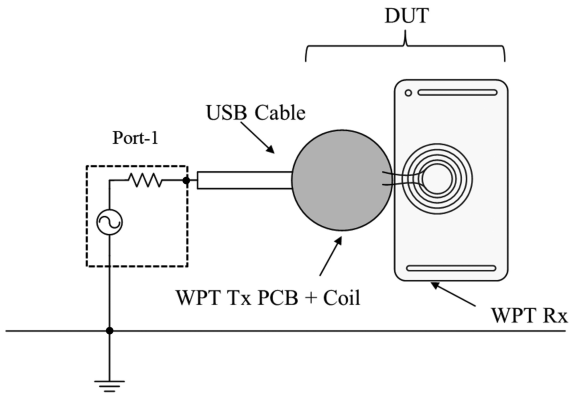

(a)

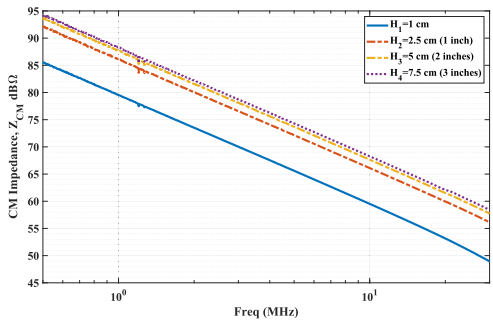

(b)

Fig. 9. CM impedance measurement of WPT module. (a) Measurement setup block diagram. (b) Measured impedance at different heights.

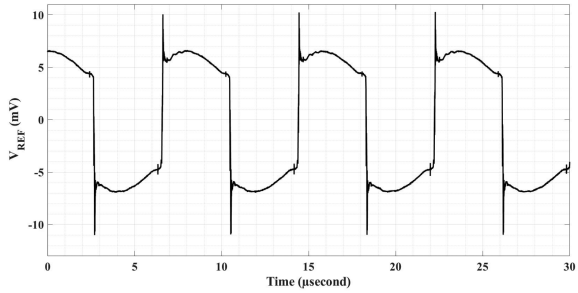

Fig. 10. Reference signal (v_{ref}) measured with H-field probe.

Z_{CM} of the WPT, the source and drain terminals of each metal-oxide-semiconductor field-effect-transistor (MOSFET) constituting the full-bridge inverter were intentionally shorted out. By electrically connecting the source and drain terminals of each MOSFET, the power and ground layers on the PCB were also considered in the Z_{CM} measurement process. The impedance Z_{CM} was measured at different heights from the ground plane: 1, 2.5 (1 in), 5 (2 inches), and 7.5 cm (3 inches). The height of the WPT system with respect to the ground plane was varied by modifying the height of the spacer (styrofoam). Fig. 9(b) shows the Z_{CM} of the WPT at different heights with respect to the ground plane. In applications where the impedance between the DUT and the ground plane is higher than the dynamic range of the VNA, a dielectric material with a dielectric constant (ε_r) greater than 1 can be used instead of styrofoam.

IV. Validation of the Three-Terminal Model

The measurement setup shown in Fig. 4 was used to extract a setup independent terminal model of a WPT system (or any power converter) described in Section I. The currents i_1, i_2, i_3, i_4, i_5, and i_6 were obtained by measuring the voltages at Probe_P and Probe_N locations in Fig. 6 and using (10) and (11). Rohde and Schwarz RT2024 [12] oscilloscope was used for the measurements. The currents measured in the time domain were converted to the frequency domain data using the fast Fourier transforms (FFT), as shown in (11) and (12). A total of 64 averages was used to suppress the random behavior in the signal. To perform the averages, the trigger on the oscilloscope was set on the V_{REF} channel. The reference signal voltage,V_{REF}, was measured using the H-field probe placed close to the phase output of the inverter. The V_{REF} signal was also used to correct the phase of the voltages or currents measured at the outputs (12). An example of V_{REF} is shown in Fig. 10. A total of 1 ms of time-domain data with 1 GS/s was obtained using an oscilloscope.

As discussed in Section II, each measurement produces a set of two equations, and five equations are required to extract the unknowns: V_{P}, V_{N}, Z_{P}, Z_{N}, and Z_{PN}. A combination of different impedances ($Z_{\mathbf{C\_load}}$) are used to obtain various currents in (3)–(8). A $Z_{\mathrm{C\_load}}$ value of 50, 150, and 450 Ω was used for extraction when the WPT was placed 1 in above the ground plane. An example of the voltage measured on the P-line is shown in Fig. 11. Here, the $Z_{\mathrm{C\_load}}$ is varied between 150 and 450 Ω, respectively, and height $H_1 = 1$ in. As can be observed in

Authorized licensed use limited to: Missouri University of Science and Technology. Downloaded on August 29,2023 at 13:58:31 UTC from IEEE Xplore. Restrictions apply.

This article has been accepted for inclusion in a future issue of this journal. Content is final as presented, with the exception of pagination.

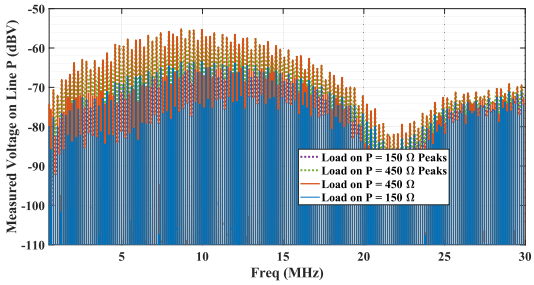

Fig. 11. Measured voltages V_1 and V_2 on the P-line along with their peaks, where R_{load}= 150 and 450 Ω, respectively.

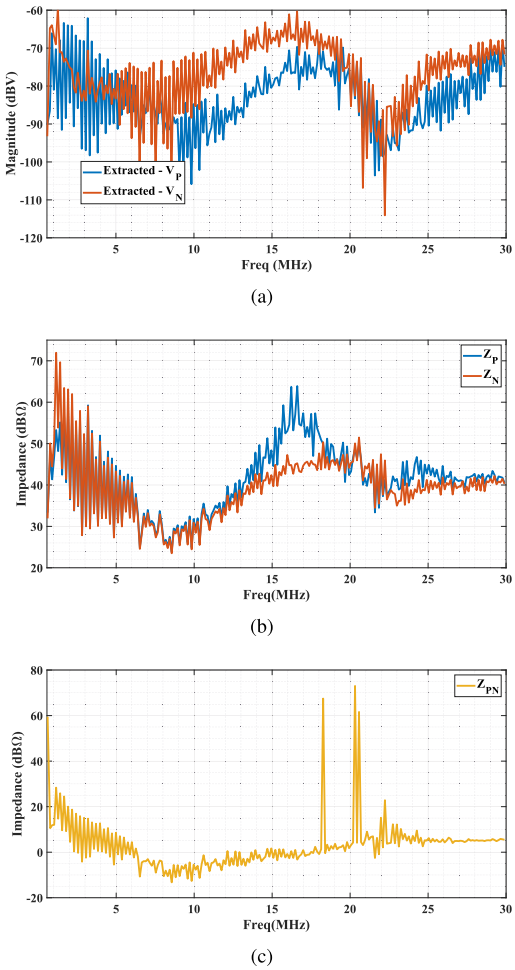

Fig. 12. Extracted sources for the WPT: (a) V_{P}, V_{N}, (b) Z_{P}, Z_{N}, and (c) Z_{PN}.

Fig. 11, the variation in the voltages is at least 2 to 10 dB, enough resolution for the equations to be solved without converging to a single value. A similar observation was made on the N-line, although not shown here. Fig. 12 shows the extracted sources using the abovementioned $Z_{\text{C\_load}}$ impedances.

$$|I_i|\, e^{j\varphi} = \text{FFT}\,(i_i) \tag{11}$$

$$|V_{\text{REF}i}|\, e^{j\varphi} = \frac{\text{FFT}(i_i)}{\text{FFT}\,(v_{\text{ref}i})} \tag{12}$$

where $i = 1, 2, 3 \ldots 6$. where I_7 and I_8 are predicted currents for the load impedance of Z''_{LP}, Z''_{LN}, and CM impedance of Z''_{CM}.

TABLE I
VARIOUS HEIGHTS AND LOADS USED FOR SOURCE EXTRACTION AND CM CURRENT AND VOLTAGE PREDICTION

	$Z_{\text{C\_load\_P}}$ (Ω)	$Z_{\text{C\_load\_N}}$ (Ω)	Height (inches)
Extraction	50	50	1
	150	150	1
	450	450	1
Prediction	350	350	1
	350	100	2

Equation (13) shown at the bottom of the next page, was used to verify the extracted terminal model of the WPT system, along with the setup shown in Fig. 4. The verification was performed for two different conditions. In the first step, the setup used for extraction was used for prediction, but the $Z_{\text{C\_load}} = 350\ \Omega$. Fig. 13 shows the comparison of the measured and predicted currents on the P and N lines. In another case, the $Z_{\text{C\_load}}$ on the P line was 350 Ω and N was 100 Ω—a case where the P and N lines were terminated with different impedances. To demonstrate the setup-independent nature of the extracted sources, the WPT was placed 2 in above the ground plate in the latter case (see Fig. 14). In both cases, a maximum of 4 dB error was achieved between measurements and prediction. Table I describes the different loads used for extraction of the sources and prediction.

In the next step, a 1-m cable harness (a twisted pair) was connected to the WPT. Both the WPT system and cable harness are placed 2 in above the ground plane. The cable harness is connected to the power supply through the LISN. The voltage on the P and N lines are measured at the output of the LISNs. The S-parameters of the cable harness are extracted using VNA (see Fig. 15). A two-port VNA was used to obtain the four-port S-parameters of the cable harness. All the unused ports during the measurement process were terminated with 50 Ω termination. Only one measurement setup is shown in Fig. 15 (S_{11}, S_{22}, and S_{12}) while other measurement setups are similar. The vertical copper plates connecting the two ends of the cable prevent unwanted inductance caused by the VNA ports and the cable harness terminals. During the verification process, the S-parameters of the cable harness were cascaded with the extracted source from Fig. 4. The circuit simulation tool Keysight ADS [13] was used during this process. Fig. 16 shows the ADS circuit model for predicting the voltages at the output of the P and N LISNs. The output voltages are marked with black dashed lines in Fig. 16. The LISN was also replaced with its circuit model (see Fig. 7) in the final simulation, including the LISN parasitic impedances. These parasitic impedances were obtained by tuning the parasitic capacitance, inductance, and resistance associated with the LISN components to match the Z-parameters of the LISN circuit (see Fig. 7) model and the Z-parameters of the measurements performed using Fig. 8(a). Fig. 17 shows a comparison of measured voltage conducted emission, V_{CE}, and predicted voltage. The $Z_{\text{C\_load}}$ used here is 350 Ω.

V. CONDITIONS FOR VALIDITY OF THE EXTRACTED SOURCE

The extracted three-terminal source information is valid only under certain conditions because the multiterminal model provides a linear terminal model for nonlinear switching devices

Authorized licensed use limited to: Missouri University of Science and Technology. Downloaded on August 29,2023 at 13:58:31 UTC from IEEE Xplore. Restrictions apply.

This article has been accepted for inclusion in a future issue of this journal. Content is final as presented, with the exception of pagination.

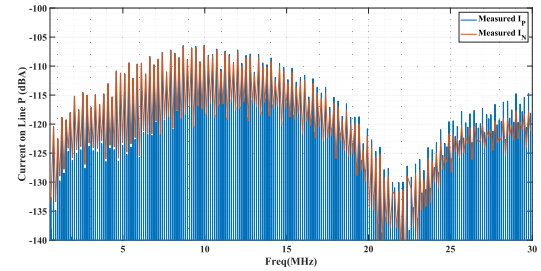

(a)

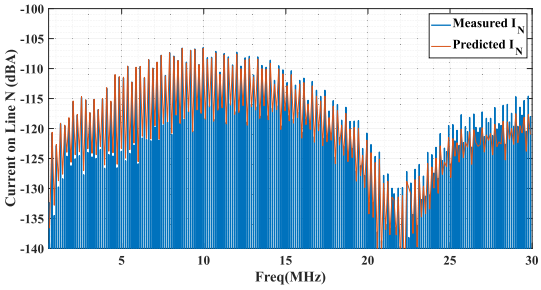

(b)

Fig. 13. Comparison of predicted and measured currents with $R_{\text{load}} = 350\ \Omega$ on the P and N lines and WPT 1-in above the ground plane. (a) Current on P. (b) Current on N.

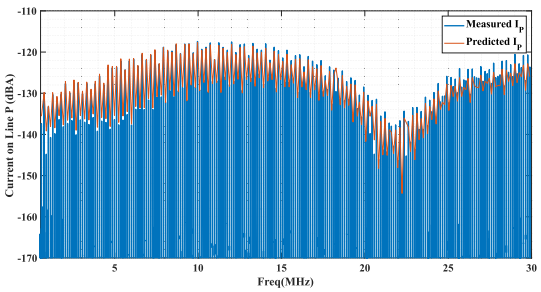

(a)

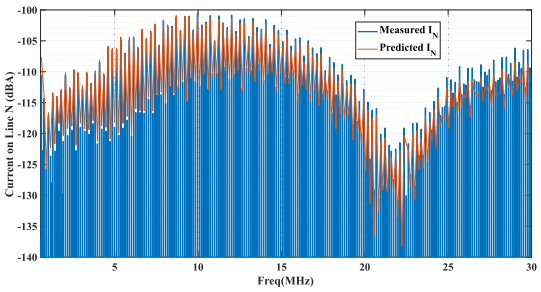

(b)

Fig. 14. Comparison of predicted and measured currents with $R_{\text{load}} = 350\ \Omega$ on P and $R_{\text{load}} = 100\ \Omega$ on N lines when the WPT is 2 in above the ground plane. (a) Current on P. (b) Current on N.

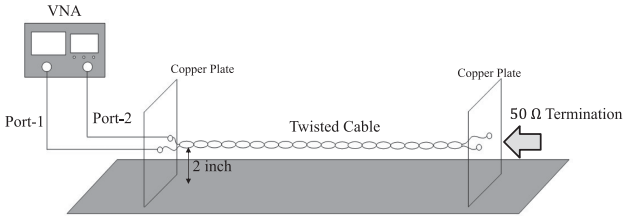

Fig. 15. Example measurement for extracting S-parameters using a two-port VNA. The example shows measurement of S_{11}, S_{22}, and S_{12}.

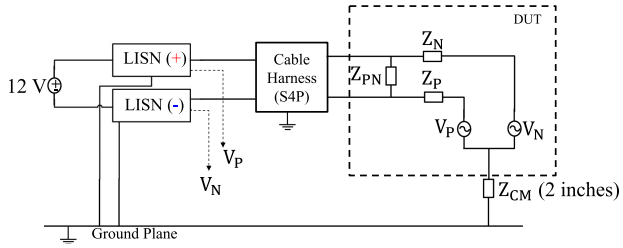

Fig. 16. Circuit simulation model for predicting V_{CE} using three-terminal model.

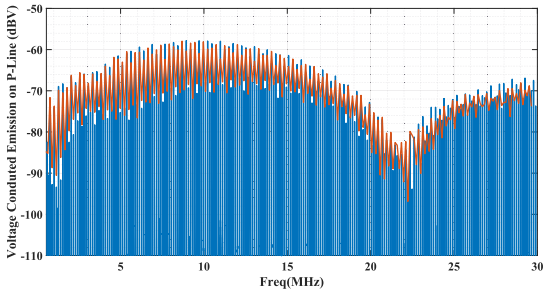

(a)

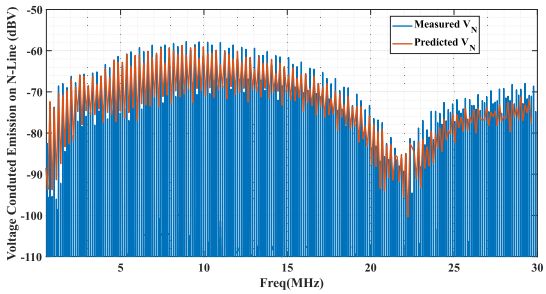

(b)

Fig. 17. Comparison of predicted and measured V_{CE} with cable harness and $R_{\text{load}} = 350\ \Omega$ on the P and N lines, WPT is 2 in above the ground plane. (a) V_{CE} P. (b) V_{CE} on N.

(MOSFETs), as stated in Section III. The first condition: throughout the this article, the WPT Rx coil was fixed in position with respect to the WPT Tx coil. Fig. 18 shows an example of the variation in the peak values of the currents on the P-line when the WPT Rx position was varied between two different positions.

$$\begin{bmatrix} I_7 \\ I_8 \end{bmatrix} = \begin{bmatrix} \left(Z_{\text{P}} + Z_{\text{P}}\frac{Z''_{\text{LP}}}{Z_{\text{PN}}} + Z''_{\text{LP}} + Z''_{\text{CM}}\right) & -\left(Z''_{\text{LN}}\frac{Z_{\text{P}}}{Z_{\text{PN}}} - Z''_{\text{CM}}\right) \\ -\left(Z_{\text{N}}\frac{Z''_{\text{LP}}}{Z_{\text{PN}}} - Z_{\text{CM}}\right) & \left(Z_{\text{N}} + Z_{\text{N}}\frac{Z''_{\text{LP}}}{Z_{\text{PN}}} + Z_{\text{LN}} + Z_{\text{CM}}\right) \end{bmatrix} \begin{bmatrix} V_{\text{P}} \\ V_{\text{N}} \end{bmatrix} \tag{13}$$

Authorized licensed use limited to: Missouri University of Science and Technology. Downloaded on August 29,2023 at 13:58:31 UTC from IEEE Xplore. Restrictions apply.

This article has been accepted for inclusion in a future issue of this journal. Content is final as presented, with the exception of pagination.

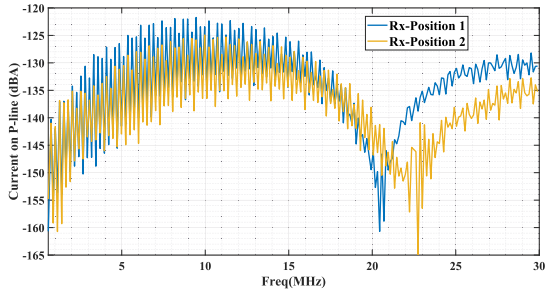

Fig. 18. Comparison of peak values of the measured currents on the P-line when the WPT Rx position was changed between two different positions.

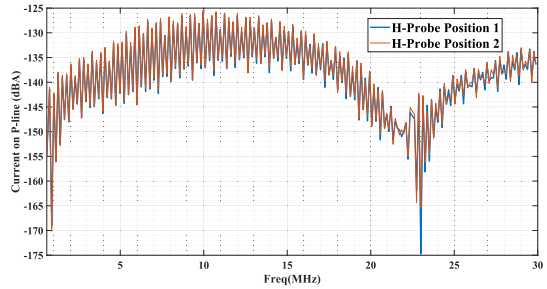

Fig. 19. Comparison of peak values of the measured currents on the P-line when the H-field probe position was changed between different positions.

Only peak current values are shown in Fig. 18 for clarity. Significantly more error was seen here than in earlier examples; hence, the extracted three-terminal source information is valid only when the Rx coil is fixed in the same position as used for extraction. For applications where the maximum noise is to be predicted, the position of the Rx-coil can be fixed where CM noise is the maximum. For applications where the maximum noise is to be predicted, the position of the Rx-coil can be fixed where CM noise is the maximum.

In the second condition, the $Z_{\text{C\_load}}$ values used throughout the paper are 50, 150, 350, and 450 Ω. The three-terminal model is valid only when the WPT system is terminated with values of $Z_{\text{C\_load}}$ between 50 and 450 Ω.

The position of the H-field probe used for measuring the reference voltage V_{REF} was also changed to verify if there is a path between the switching node of the full H-bridge on the WPT Tx PCB and the H-field probe that affects the measurements. As seen from Fig. 19, the position of the H-field probe does not affect the measurement. While Figs. 18 and 19 only show the peak current on the P-line, a similar conclusion can be drawn for the N-line as well.

VI. Conclusion

A setup-independent three-terminal model for predicting emissions from power converters was proposed in this article. A Qi-based WPT system was used as the DUT to verify the proposed method. The buck converter and full-bridge inverter are the main noise sources on the DUT, causing DM and CM currents to flow on the cable harness connected to the DUT. First, a methodology to separate the extracted three-terminal noise sources from setup configuration was discussed. This was achieved by introducing a known Z_{CM} into the circuit model. A total of six nonlinear equations are solved to extract the unknowns of the terminal model. Next, a measurement setup describing the measurement of currents and voltages required to extract the source information was introduced. Once the sources $V_{\text{P}}, V_{\text{N}}, Z_{\text{P}}, Z_{\text{N}},$ and Z_{PN} were extracted, these were verified on a setup that was different from the setup used to extract the sources. The change in the setup was achieved by modifying the termination impedance to 350 Ω as well as modifying the height of the DUT with respect to the ground plane. In the final step, the extracted sources were used to predict the conducted emissions on a 1-m long cable harness. In the abovementioned scenarios, the predicted conducted emissions predicted the envelope of the measured emissions within 5 dB.

References

[1] C. Song et al., "Three-phase magnetic field design for low EMI and EMF automated resonant wireless power transfer charger for UAV," in *Proc. IEEE Wireless Power Transfer Conf.*, 2015, pp. 1–4.

[2] C. Kim, D. Seo, J. You, J. Park, and B. H. Cho, "Design of a contactless battery charger for cellular phone," *IEEE Trans. Ind. Electron.*, vol. 48, no. 6, pp. 1238–1247, Dec. 2001.

[3] H. Bishnoi, A. C. Baisden, P. Mattavelli, and D. Boroyevich, "Analysis of EMI terminal modeling of switched power converters," *IEEE Trans. Power Electron.*, vol. 27, no. 9, pp. 3924–3933, Sep. 2012.

[4] A. C. Baisden, "Generalized terminal modeling of electro-magnetic interference," Ph.D. dissertation, Dept. Elect. Eng., Virginia Tech, Blacksburg, VA, USA, 2010.

[5] L. Ran, J. C. Clare, K. J. Bradley, and C. Christopoulos, "Measurement of conducted electromagnetic emissions in PWM motor drive systems without the need for an LISN," *IEEE Trans. Electromagn. Compat.*, vol. 41, no. 1, pp. 50–55, Feb. 1999.

[6] H. Bishnoi, P. Mattavelli, R. Burgos, and D. Boroyevich, "EMI terminal modeling of DC-fed motor drives," in *Proc. 15th Eur. Conf. Power Electron. Appl.*, 2013, pp. 1–10.

[7] S. Shinde et al., "Radiated EMI estimation from DC–DC converters with attached cables based on terminal equivalent circuit modeling," *IEEE Trans. Electromagn. Compat.*, vol. 60, no. 6, pp 1769–1776, Dec. 2018.

[8] T. Makharashvili et al., "Prediction of common mode current in cable harnesses," in *Proc. IEEE Int. Symp. Electromagn. Compat. IEEE Asia-Pacific Symp. Electromagn. Compat.*, 2018, pp. 321–326.

[9] A. PÉrez, A.-M. SÁnchez, J.-R. ReguÉ, M. RibÓ, P. Rodróguez-Cepeda, and F.-J. Pajares, "Characterization of power-line filters and electronic equipment for prediction of conducted emissions," *IEEE Trans. Electromagn. Compat.*, vol. 50, no. 3, pp. 577–585, Aug. 2008.

[10] G. Shen et al., "Terminal modeling of DC–DC converters with stochastic behavior," *IEEE Trans. Electromagn. Compat.*, vol. 60, no. 6, pp. 2011–2018, Dec. 2018.

[11] "Solve nonlinear least-squares (nonlinear data-fitting) problems," [Online]. Available: https://www.mathworks.com/help/optim/ug/lsqnonlin.html

[12] Rohde and Schwarz RT2024, "R&S®RTO2000 oscilloscope | Rohde & Schwarz," [Online]. Available: rohde-schwarz.com

[13] Keysight ADS. [Online]. Available: https://www.keysight.com/us/en/products/software/pathwave-designsoftware/pathwave-advanced-design-system.html

Authorized licensed use limited to: Missouri University of Science and Technology. Downloaded on August 29,2023 at 13:58:31 UTC from IEEE Xplore. Restrictions apply.